Available online www.jocpr.com

Journal of Chemical and Pharmaceutical Research, 2013, 5(10):289-305

Research Article

ISSN : 0975-7384
CODEN(USA) : JCPRC5

Synthesis of thiazole based 1,3,4-oxadiazole derivatives and their corrosion inhibition characteristics at mild steel/hydrochloric acid interface

C. B. Pradeep Kumar and K. N. Mohana*

Department of Studies in Chemistry, University of Mysore, Manasagangotri, Mysore, India

---

ABSTRACT

4-(((4-((5-Mercapto-1,3,4-oxadiazol-2-yl)methyl)-5-methylthiazol-2-yl)imino)methyl)benz ene-1,2-diol ***(5a)*** *and 4-(((4-((5-Mercapto-1,3,4-oxadiazol-2-yl)methyl)-5-methylthiazol-2-yl)imino)methyl)-2,6-dimethoxyphenol* ***(5b)*** *are synthesized and their structures have been confirmed by IR and ^{1}H-NMR spectral studies. Antioxidant activity of the synthesized compounds was investigated, and corrosion inhibition behaviour of the synthesized compounds on mild steel in 0.5 M HCl was studied by mass loss and electrochemical techniques. Thermodynamic adsorption parameters indicated both physisorption as well as chemisorption mechanism, and the process followed Langmuir adsorption isotherm. The polarization curves showed that both the compounds act as mixed type of inhibitor. FTIR spectra and scanning electron microscopy (SEM) were used to analyze the surface adsorbed film.*

Keywords: Oxadiazole; Antioxidant activity; Polarization; Electrochemical impedance spectroscopy (EIS); FTIR spectra; SEM

INTRODUCTION

Corrosion of iron and its alloys has been a subject of numerous studies due to their wide range of industrial applications. Mild steel (MS) is one of the well known engineering structural material used in chemical processing, petroleum production, refining, pipelines, mining, construction, etc., due to its excellent mechanical properties and low cost. One of its shortcomings is that it undergoes corrosion in various operating environments such as addition of acids for the removal of undesirable scale and rust in many industrial processes. Crude oil is corrosive to MS which is widely used in the petroleum industry. About 25 – 30 % of the total economic losses in the oil and natural gas industries are due to failure of pipes and other plants resulting from metallic corrosion [1–3].

Despite continuing advances in the formulation of corrosion resistance materials, the use of chemical corrosion inhibitors often remains the most practical and cost effective way of preventing corrosion. The use of organic inhibitors for preventing corrosion is a promising alternative solution [4-7]. The choice of effective inhibitors is based on their mechanism of action and their electron donating capability. The inhibiting ability of the inhibitor is supported by molecular structure of the adsorption active sites with lone pair and/or *p* - orbitals such as heterocyclic rings containing sulphur, oxygen, phosphorus and/or nitrogen atoms [8–10]. They have an ability to accept or donate electrons in order to be adsorbed on metallic surfaces by electrostatic interaction between the unshared electron pair of corrosion inhibitor and metal. These inhibitors are usually adsorbed on the metal surface by the formation of a coordinate covalent bond (chemical adsorption) or the electrostatic interaction between the metal and inhibitor (physical adsorption) [11].

Oxadiazole derivatives offer special affinity to inhibit corrosion of metals in different aggressive environments [12-16], and as potent antioxidant substances [17-19]. These compounds rich in heteroatoms can be regarded as environmental friendly inhibitors because of their strong chemical activity and low toxicity [20-21]. Thus in the light of above, we undertook the examination of antioxidant activity and corrosion inhibition behaviour of the newly synthesized compounds, 4-(((4-((5-Mercapto-1,3,4-oxadiazol-2-yl)methyl)-5-methylthiazol-2-yl) imino) methyl) benzene-1,2-diol **(5a)** and 4-(((4-((5-Mercapto-1,3,4-oxadiazol-2-yl)methyl)-5-methylthiazol-2-yl)imino)methyl) -2,6-dimethoxyphenol **(5b)**. The synthesized compounds were characterized by FTIR, elemental analyses and ^{1}H-NMR spectral studies. Antioxidant activity was studied by assaying diphenylpicrylhydrazyl (DPPH), nitric oxide and hydroxyl radicals. Mass loss and electrochemical techniques were used to elucidate the corrosion inhibition mechanism of **5a** and **5b** on MS in 0.5 M HCl. The thermodynamic activation and adsorption parameters were calculated and discussed.

EXPERIMENTAL SECTION

2.1 Materials and Solutions

The specimens used for corrosion tests were mild steel (MS) coupons which have the following composition (wt %): 0.051 C: 0.023 Si: 0.005 P: 0.103 Al: 0.179 Mn: 0.023 S and the remainder iron. Before gravimetric and electrochemical measurements, the surface of the specimens was polished under running tap water using emery paper (SiC, grade 1200 - 1600), rinsed with distilled water, dried on a clean tissue paper, immersed in benzene for 5 s, dried and immersed in acetone for 5 s, and dried with clean tissue paper. Finally, the specimens were kept in desiccators until use. At the end of the gravimetric experiment, the specimens were carefully washed with acetone and benzene, dried, and then weighed. For polarization and electrochemical impedance studies, the MS specimen was embedded in epoxy resin to expose a geometrical surface area of 1cm^2 to the electrolyte. A stock solution of inhibitor was prepared by weighing an appropriate amount of it and dissolved in 0.5 N HCl, and series of concentrations were prepared from this stock solution. Doubly distilled water was used throughout the experiment.
For the synthesis of inhibitors, all solvents and reagents were purchased from Sigma Aldrich Chemicals Pvt Ltd. Melting range was determined by Veego Melting Point VMP III apparatus. Elemental analyses were recorded on VarioMICRO superuser V1.3.2 Elementar. The FT-IR spectra were recorded using nujal on FT-IR Jasco 4100 infrared spectrophotometer. ^{1}H NMR spectra were recorded on Bruker DRX-500 spectrometer at 400 MHz using DMSO-d_6 as solvent and TMS as an internal standard.

2.2. Synthesis of inhibitors

2.2.1. Synthesis of ethyl 2-(2-amino-5-methylthiazol-4-yl) acetate (2) **[22]**

Yield: 74 %. IR (nujol, cm^{-1}): 3407 (NH_2), 1684(C=O), ^{1}H NMR (DMSO-d_6, δ ppm): 6.91 (s, 2H, NH_2), 4.07 (q, 2H, O-CH_2-CH_3), 3.43 (s, 2H, CO-CH_2), 2.32 (s, 3H, CH_3), 1.18 (t, 3H, O-CH_2-CH_3). Anal. Calcd. (%) for $C_8H_{12}N_2O_2S$: C- 47.98, H- 6.04, N- 13.99. Found (%): C- 48.02, H- 6.08, N- 14.02.

2.2.2. Synthesis of 2-(2-amino-5-methylthiazol-4-yl) acetohydrazide (3) **[23]**

Yield: 74 %. IR (nujol, cm^{-1}): 3316, 3148 (NH, NH_2), 2352 (NH_2). ^{1}H NMR ($CDCl_3$, δ ppm): 9.02 (s, 1H, NH), 6.86, 6.21 (s, 4H, 2 NH_2), 3.17 (s, 2H, CO-CH_2), 2.31 (s, 3H, CH_3), 2.19 (s, 2H, NH_2). Anal. Calcd. (%) for $C_6H_{10}N_4OS$: C - 38.70, H - 5.41, N - 30.08. Found (%): C - 38.74, H - 5.44, N - 30.78.

2.2.3. Synthesis of 2-((2-amino-5-methylthiazol-4-yl) methyl) oxadiazole-5-thiol (4) **[24]**

Yield: 70 %. IR (nujol, cm^{-1}): 3368 (NH_2). ^{1}H NMR ($CDCl_3$, δ ppm): 13.02 (s, 1H, SH), 7.05 (s, 1H, Ar-H), 6.45 (s, 2H, NH_2), 3.91 (s, 2H, CH_2), 2.31 (s, 3H, CH_3). Anal. Calcd. (%) For $C_7H_8N_4O_4S_2$ (%): C - 36.83, H - 3.53, N - 24.54. Found (%): C - 36.89, H - 3.58, N - 24.59.

2.2.4. Synthesis of 4-((4-((5-mercapto-1,3,4-oxadiazol-2-yl)methyl)-5-methylthiazol-2-ylimino)methyl)benzene-1,2-diol (5a)

Compound **4** (2 mmol) with 3,4-dihydroxybenzaldehyde (2 mmol) in methanol (30 mL), and 2 to 3 ml of glacial acetic acid was refluxed for 6 h. The reaction mixture was cooled by adding ice water the formed precipitate was filtered off, washed with water and crystallized from ethanol to obtain the desired Schiff base. Yield: 71 %, M. R (°C): 141-143, IR (nujal, cm^{-1}): 3416 (OH), 1574 (-CH=N-), ^{1}H NMR ($CDCl_3$, δ ppm): 13.05 (s, 1H, SH), 9.13 (s, 2H, 2OH), 8.62 (s, 1H, -CH=N-), 7.35-6.85 (m, 3H, Ar-H), 3.61 (s, 2H, CH_2), 2.32 (s, 3H, CH_3). MS, m/z: 349 (M+1). Anal. Calcd. (%) for $C_{14}H_{12}N_4O_3S_2$ (%): C - 48.26, H - 3.47, N - 16.08. Found (%): C - 48.32, H - 3.52, N - 16.11.

2.2.5. Synthesis of 4-((4-((5-mercapto-1,3,4-oxadiazol-2-yl)methyl)-5-methylthiazol-2-ylimino)methyl)-2,6-dimethoxy phenol (5b)

Compound **4** (2 mmol) with 4-hydroxy-3,5-dimethoxybenzaldehyde (2 mmol) in methanol (30 mL), and 2 to 3 ml of glacial acetic acid was refluxed for 6 h. The reaction mixture was cooled by adding ice water the formed precipitate was filtered off, washed with water and crystallized from ethanol to obtain the desired Schiff base. Yield: 79 %, M. R (°C): 200-202, IR (nujal, cm^{-1}): 3426 (OH), 1603 (-CH=N-). ^{1}H NMR ($CDCl_3$, δ ppm): 13.05 (s, 1H, SH), 9.13 (s, 1H, OH), 8.62 (s, 1H, -CH=N-), 7.08 (s, 2H, Ar-H), 3.83 (s, 6H, 2 OCH_3), 3.61 (s, 2H, CH_2), 2.30 (s, 3H, CH_3). MS, m/z: 393 (M+1). Anal. Calcd. (%) For $C_{16}H_{16}N_4O_4S_2$ (%): C - 48.97, H - 4.11, N - 14.28. Found (%): C - 48.93, H - 4.08, N - 14.31.

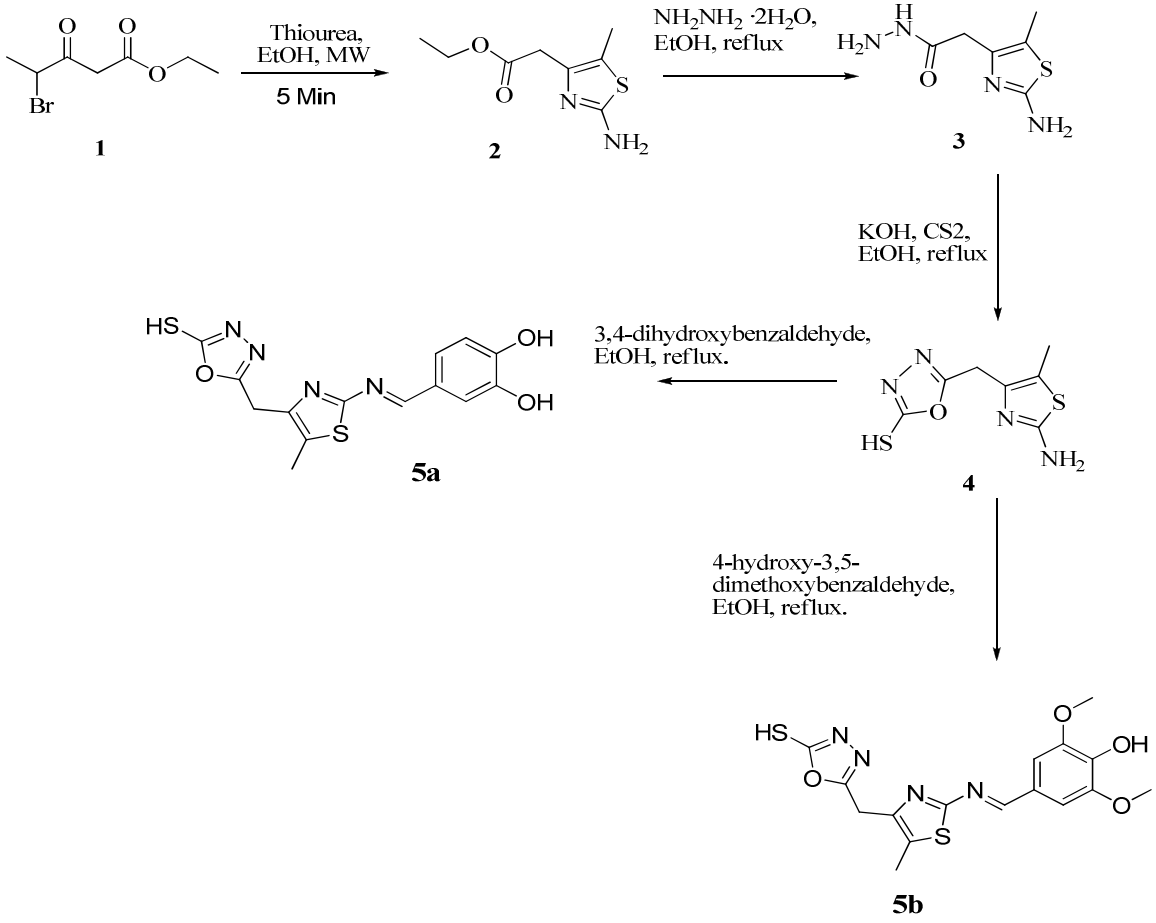

Figure 1. Scheme for the synthesis of oxadiazoles

2.3.1. Antioxidant activity

The antioxidant activity of the synthesized compounds **5a** and **5b** was determined by DPPH, hydroxyl and nitric oxide radicals scavenging assay methods [25-27] using ascorbic acid (AA) and butylated hydroxyanisole (BHA) as standards.

2.3.2. Mass loss measurements

Gravimetric experiments were carried out in a glass cell and the solution volume was 100 cm^3. The temperature of the environment was maintained by thermostatically controlled water bath (Weiber, India) with an accuracy of ± 0.2 °C under aerated condition. The MS specimens used were rectangular with a dimension of 1 cm × 1 cm × 0.1 cm. The initial weight of the specimen was recorded using an analytical balance (precision ± 0.1 mg). After the corrosion test in 0.5 M HCl with and without inhibitor, the specimens were carefully washed in double distilled water, dried and then weighed. The weight loss of the specimen was determined after an immersion period of 4 h at the temperature range of 303 to 333 K. Triplicate experiments were performed in each case and the average mass

loss was reported. The corrosion rate (C_R) and percentage inhibition efficiency symbolized as η(%) are calculated using the expressions (1) and (2).

$$C_R = \frac{\Delta W}{St} \quad (1)$$

$$\eta(\%) = \frac{(C_R)_a - (C_R)_p}{(C_R)_a} \times 100 \quad (2)$$

where, ΔW is the weight loss, S is the surface area of the specimen (cm^2) , t is the immersion time (h), and $(C_R)_a$ and $(C_R)_p$ are corrosion rates in the absence and presence of the inhibitor, respectively.

***2.3.3. Electrochemical impedance spectroscopy* (EIS)**

The EIS tests were performed in a three electrode assembly CH1660D instrument. The cell arrangement used was a conventional three-electrode cell with platinum counter electrode, saturated calomel electrode as reference electrode and test material (MS) as working electrode. All potentials are reported vs. SCE. And the measurements were done after 30 min of immersion in the test solution. EIS measurements were performed with a frequency range of 10 kHz to 0.1 Hz and amplitude of 0.005 V. The percentage inhibition efficiency η(%) was calculated using the charge transfer resistance as follows:

$$\eta(\%) = \frac{1/(R_p)_a - 1/(R_p)_p}{1/(R_p)_a} \times 100 \quad (3)$$

where, $(R_P)_a$ and $(R_P)_p$ are charge transfer resistances in the absence and presence of inhibitor, respectively.

2.3.4. Potentiodynamic polarization

The electrochemical character of MS sample in uninhibited and inhibited solutions was investigated by recording anodic and cathodic polarization curves in 0.5 M HCl solutions with different inhibitor's concentrations with an exposed area of $1cm^2$. A conventional three electrode cell consisting of MS as working electrode, platinum foil as counter electrode and saturated calomel electrode as reference electrode was used. Potentiodynamic polarization curves were recorded after immersion of the working electrode (MS) for 30 min in 0.5 M HCl solution containing different concentrations of the inhibitors in the potential range from -100 to -900 mV with a scan rate of 0.4 mV s^{-1}. The linear Tafel segments of anodic and cathodic curves were extrapolated to corrosion potential (E_{corr}) to obtain corrosion current densities (i_{corr}). The η(%) at different inhibitors concentrations are calculated using the following equation (2):

$$\eta(\%) = \frac{(i_{corr})_a - (i_{corr})_p}{(i_{corr})_a} \times 100 \quad (4)$$

where, $(i_{corr})_a$ and $(i_{corr})_p$ are the corrosion current density (μA cm^{-2}) in the absence and presence of the inhibitors, respectively.

2.3.5. SEM and FTIR studies

The surface morphology of the MS samples in the absence and presence of **5a** and **5b** was investigated by Scanning Electron Microscopy (SEM) technique (Model JSM-5800). The surface products deposited on the test specimens with inhibitors after 5 h of exposure in the 0.5 M HCl were analyzed by FTIR spectrophotometer.

RESULTS AND DISCUSSION

3.1. Antioxidant activity

The *in-vitro* antioxidant activity of compounds **5a** and **5b** were determined spectrophotometrically by DPPH method and the results are given in Table 1. DPPH radicals are stable free radicals, and in the presence of molecules capable of donating H atoms, its radical character is neutralized [28]. The reduction capacity of DPPH radicals was determined by the decrease in its absorbance at 517 nm, which is induced by antioxidants. On the other hand, it is well-established that organic molecules incorporating an electron donating group (amine, hydroxyl and methoxy)

can act as free radical trapping agents and are capable of opposing oxidative challenges. It can be seen from Table 1 that compounds **5a** and **5b** present the good scavenging activity on DPPH$^{\bullet}$. The compounds bearing a hydroxyl group (electron donating group) at para position showed dominate DPPH activity with an IC_{50} value of 13.5 and 14.0 µg/mL, respectively.

The synthesized compounds were also screened for hydroxyl radical and nitric oxide scavenging assays. Hydroxyl radical (·OH) scavenging capacity of the compound is directly related to its antioxidant activity as depicted in Table 1. The compounds **5a** and **5b** are found to show better inhibition with IC_{50} 14.8 and 17.01 µg/mL, respectively, compared with standard BHA (15.3 µg/mL). Compounds **5a** and **5b** inhibit nitric oxide with IC_{50} values of 14.3±0.11 µg/ml and 16.0±0.38 µg/ml. The IC_{50} value of **5a** is less than that of the standard (14.8±0.19 µg/ml), where as IC_{50} value of **5b** is greater than that of standard.

3.2. Antioxidant activity and corrosion inhibition

Antioxidants from natural sources have high bioavailability, therefore high protective efficiency against free radicals [29]. Free radicals and singlet oxygen scavengers (antioxidants) were found to have metal and alloy corrosion inhibition character, which depend to a greater extent on the structural feature of the antioxidant added and to its accepting - donating hydrogen or electron behaviors [30]. In this connection, and on the basis of available results obtained by antioxidant activity measurements, we undertook examination of corrosion inhibition studies of compounds **5a** and **5b**. The results showed that compounds **5a** and **5b** are good corrosion inhibitors with maximum inhibition efficiency η(%) values of 87.88 % and 80.00 %, respectively. Greater antioxidant activity and corrosion inhibition behaviour of compound **5a** is linked to the electron donating effect of the two hydroxyl groups attached to aromatic ring, which increases the electron density on the benzene ring. The increasing delocalization of electron density in the molecule makes more reactive towards scavenging reactive oxygen as well as inhibiting corrosion process. The adsorption of inhibitor molecules is further stabilized by participation of π electrons of benzene ring. Electronegative oxygen, sulfur and nitrogen atoms present in compounds **5a** and **5b** facilitate more efficient adsorption of the molecules on MS surface. Reduction of oxygen availability in the corroding system and the presence of a barrier between the electrode surface and oxygen retarding the rate of metal corrosion [31].

Table 1. IC_{50} values for evaluated antioxidant assays of 5a and 5b

Compounds	IC_{50} (µg/mL)		
	DPPH	HO^-	NO^-
5a	13.5±0.43	14.8±0.15	14.3±0.19
5b	14.0±0.17	17.1±0.01	16.0±0.38
AA[a]	12.6±0.43	-	-
BHA[b]	-	15.3±0.76	14.6±0.11

[a] *ascorbic acid*
[b] *butylated hydroxyanisole*

3.3. Mass loss measurements

The values of η(%) and corrosion rate obtained from weight loss method at different concentrations of the inhibitors at different temperatures are summarized in Table 2**.** It has been found that the compounds **5a** and **5b** inhibit the corrosion of MS at all studied concentrations. The corrosion rate decreased as the concentration of **5a** and **5b** increases up to 14.37×10^{-4} M and 12.76×10^{-4} M. This could be attributed to the increase in adsorption of the inhibitors onto the mild steel surface [32].

The variation of η(%) with temperature and inhibitor concentration is shown in Fig. 2a and 2b. It can be seen that η(%) at different concentrations of **5a** and **5b** causes a significant decrease with an increase in temperature from 303 - 333 K. This behavior could be attributed to decrease in the strength of the adsorption process at higher temperatures. The lone pair of electron on the nitrogen atom will co-ordinate with the metal atoms of actives sites. Also, the presence of higher electron density in the inhibitor molecules causes stronger interaction with metal surface. The nitrogen atoms can donate π electrons to the metal surface to increase adsorption and hence inhibit the corrosion process [33]. The presence of electron donating OH groups in **5a** and OCH_3 group in **5b** increases the electron density of the benzene ring. However, the OCH_3 group in **5b** increases moderately the localization of lone pair of electrons on nitrogen atoms.

Table 2. *CR* and η(%) obtained from weight loss measurements of MS in 0.5 M HCl containing various concentrations of 5a and 5b at different temperatures

Inhibitor	$C\times10^{-4}$ (M)	Temperature							
		303 K		313 K		323 K		333 K	
		C_R (mg cm^{-2} h^{-1})	η(%)	C_R (mg cm^{-2} h^{-1})	η(%)	C_R (mg cm^{-2} h^{-1})	η(%)	C_R (mg cm^{-2} h^{-1})	η(%)
5a	0	0.4276	-	0.5781	-	0.7112	-	1.2123	-
	5.75	0.1024	76.05	0.1584	72.60	0.2188	69.23	0.4404	63.67
	8.62	0.0858	79.93	0.1412	75.57	0.2008	71.76	0.4312	64.43
	11.49	0.0724	83.07	0.1162	79.90	0.1712	75.92	0.3812	68.55
	14.37	0.0518	87.88	0.0962	83.36	0.1411	80.16	0.3215	73.38
5b	5.10	0.1345	68.54	0.1992	65.54	0.2722	61.72	0.5304	56.24
	7.65	0.1164	72.78	0.1822	68.48	0.2522	64.53	0.5024	58.55
	10.20	0.1024	76.05	0.1542	73.32	0.2322	67.35	0.4504	62.84
	12.76	0.0855	80.00	0.1322	77.13	0.1922	72.97	0.3994	67.05

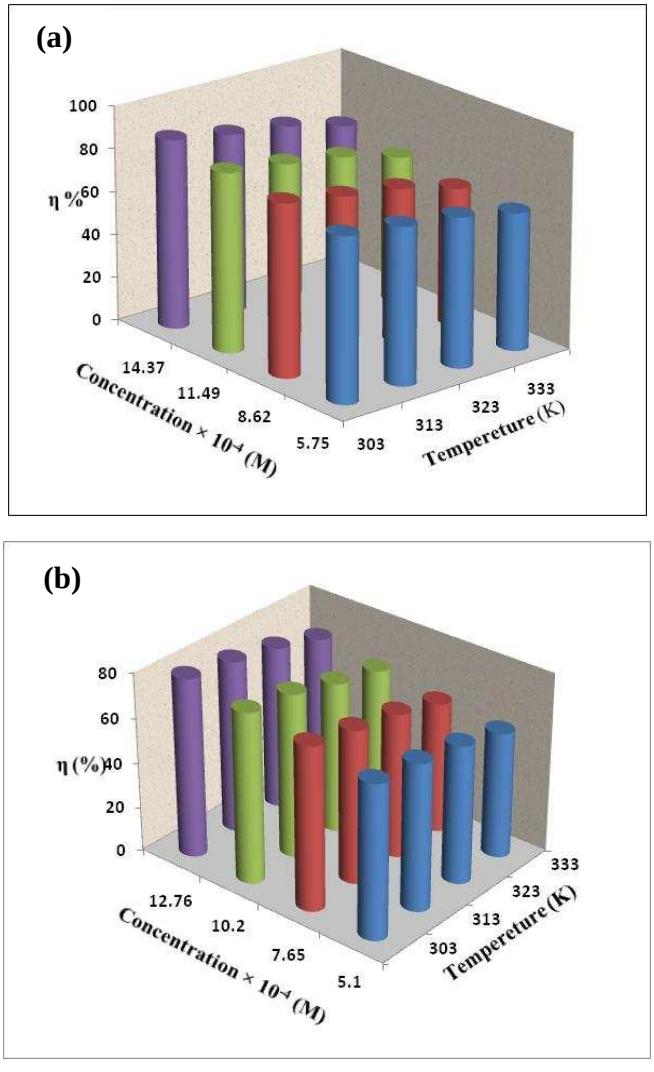

Figure 2. Variation of inhibition efficiency with temperature and inhibitor concentration in the absence and presence of different concentrations of (a) 5a (b) 5b

3.4. Effect of temperature

The activation parameters play important role in understanding the inhibitive mechanism of **5a** and **5b**. Results of η(%) obtained at different temperatures reveal that, increasing temperature increases the corrosion rate and decreases η(%). The dependence of corrosion rate on temperature can be expressed by the following Arrhenius equation:

$$C_R = A \exp\left(-\frac{E_a}{RT}\right) \quad (5)$$

where E_a is the apparent activation energy, T is the absolute temperature, A is the Arrhenius pre-exponential constant and R is the universal gas constant. The apparent activation energy and pre-exponential factor for different concentrations of the inhibitor were calculated from the plots of logarithm of *CR* versus *1/T* (Fig. 3a and 3b) and the results are shown in Table 3. It was found that higher values of E_a in the presence of inhibitors indicate more energy is required for dissolution of the MS in 0.5 M HCl [34]. This means that, the presence of inhibitor induces an energy barrier for the corrosion reaction and this barrier increases with increase in inhibitor concentration. Enthalpy and entropy of activation were calculated using the alternative form of Arrhenius equation (6):

$$C_R = \frac{RT}{Nh} \exp\frac{\Delta S}{R} \exp\left(-\frac{\Delta H}{RT}\right) \quad (6)$$

where h is Planck's constant and N is Avogadro's number, R is the universal gas constant, ΔH is the enthalpy of activation and ΔS is the entropy of activation. Using Eq. (6), plots of log (C_R/T) versus $1/T$ gave straight lines (Figs. 4a and 4b) with a slope of (- ΔH /2.303R) and an intercept of [log (R/Nh) + ΔS /2.303R]. From the plot, the values of ΔH and ΔS were calculated and tabulated in Table 3.The positive values of ΔH both in the absence and presence of **5a** and **5b** reflect the endothermic nature of the MS dissolution and it indicates that the dissolution of MS is difficult. Further, the values ΔH obtained from the Eq. (6) and those values obtained from equation, $\Delta H = E_a - RT$ are in good agreement with each other. The entropy of activation decreased in the presence of inhibitors compared to that in free acid. Such variation reflects the formation of an ordered stable film of inhibitor compounds on the MS surface [33]. Large and negative values of ΔS in uninhibited and inhibited solutions implies that the activated complex in the rate determining step represents an association rather than dissociation step, means decrease in disordering takes place on going from reactants to the activated complex [35, 36].

Table 3. Activation parameters for MS in 0.5 M HCl in the absence and presence of different concentrations of 5a and 5b

Inhibitor	$C\times10^{-4}$ (M)	E_a (kJ mol^{-1})	K (mg cm^{-2} h^{-1})	ΔH (kJ mol^{-1})	$\Delta H=E_a - RT$ (kJ mol^{-1})	ΔS (J mol^{-1}K^{-1})
5a	0	27.82	25585.86	25.17	25.30	-169.39
	5.75	39.25	568852.9	36.62	36.73	-143.59
	8.62	43.42	2488857	40.78	40.90	-131.32
	11.49	44.86	3689776	42.21	42.34	-128.14
	14.37	49.01	14157938	46.37	46.49	-116.86
5b	5.10	36.97	301300.6	34.55	34.55	-148.88
	7.65	39.38	682338.7	36.74	36.86	-142.08
	10.20	40.55	941889.6	37.91	38.03	-139.40
	12.76	41.75	1261828	39.11	39.24	-136.90

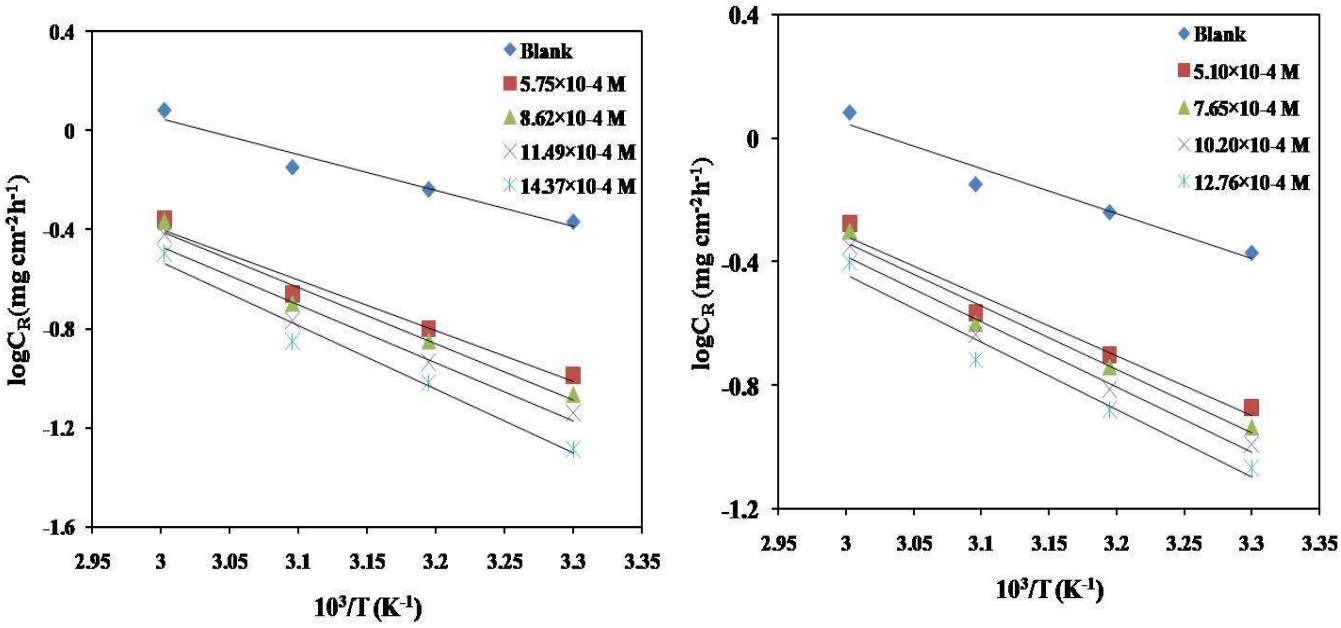

(a) (b)

Figure 3. Arrhenius plots for MS in 0.5 M HCl in the absence and presence of different concentrations of compounds (a) 5a (b) 5b

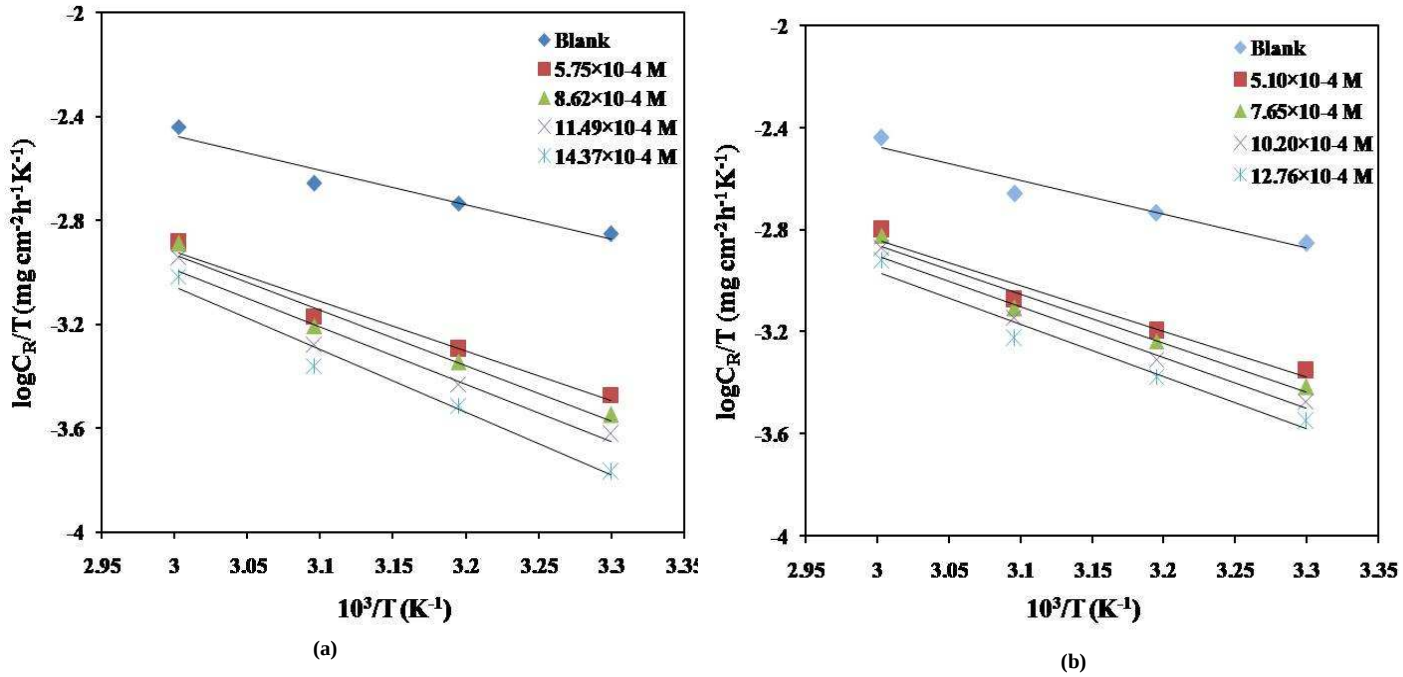

(a) (b)

Figure 4. Alternative Arrhenius plots for MS in 0.5 M HCl in the absence and presence of different concentrations of (a) 5a (b) 5b

3.5. Adsorption considerations

In order to get a better understanding of the adsorption mode of the inhibitor on the metal surface, the data were tested graphically by fitting to various isotherms to find the best isotherm which describes this study. Langmuir adsorption isotherm was found to fit well with the experimental data (Fig. 5a and 5b). The strong correlation (R^2 > 0.99) suggests that the adsorption of inhibitors on the MS surface obeyed this isotherm. According to this isotherm, θ is related to the C and equilibrium constant of adsorption K_{ads}, using equation (7):

$$\frac{C}{\theta} = \frac{1}{K_{ads}} + C \tag{7}$$

The standard free energy of adsorption (ΔG_{ads}) can be obtained using the following equation (8):

$$K_{ads} = \frac{1}{55.5} \exp\left(\frac{-\Delta G_{ads}}{RT}\right) \tag{8}$$

where R is the universal gas constant, T is the absolute temperature and 55.5 is the concentration of water in solution (mol L^{-1}). This isotherm is based on the assumption that the solid surface contains a fixed number of adsorption sites and each site holds one adsorbed species. Using equation (8), the calculated ΔG_{ads} valves are tabulated in Table 4. In general, the values of ΔG_{ads} around - 20 kJ mol^{-1} or less negative are associated with an electrostatic interaction between charged inhibitor molecules and charged electrode surface, i.e., physisorption and those of - 40 kJ mol^{-1} or more negative values involve charge sharing or transfer of electrons from the inhibitor molecules to the metal surface to form a coordinate type bond, i.e., chemisorption [37]. The calculated values of ΔG_{ads} for the studied inhibitors **5a** and **5b** are ranging from - 34.30 to - 37.07 and - 33.96 to - 36.38 kJ mol^{-1}, respectively as presented in Table 4 indicating adsorption of these inhibitors involves combination of both physisorption and chemisorptions, and similar observation was reported by Naik *et al.* [38]. The higher values of K_{ads} refer to higher adsorption and higher inhibiting effect of inhibitors [39]. The enthalpy and entropy of adsorption (ΔH_{ads} and ΔS_{ads}) can be calculated using the following equation:

$$lnK_{ads} = \ln\frac{1}{55.5} - \frac{\Delta Hads}{RT} + \frac{\Delta Sads}{R} \tag{9}$$

Using Eq. (9), the values of ΔH_{ads} and ΔS_{ads} were evaluated from the slope and intercept of the plot of $\ln K_{ads}$ versus 1/T (Fig. 6). The negative values of ΔH_{ads} (Table 4) reflect the exothermic behavior of the adsorption of inhibitors on the MS surface. The values of ΔS_{ads} are positive in the adsorption process indicating increase in solvent entropy [40]. The reason is that the adsorption of organic inhibitor molecules from the aqueous solution can be regarded as a quasi-substitution process between the organic compound in the aqueous phase [$Org_{(sol)}$] and water molecules at the electrode surface [$H_2O_{(ads)}$] [41-43]. In this situation, the adsorption of **5a** and **5b** are accompanied by desorption of water molecules from the electrode surface. The positive values of ΔS_{ads} suggest that gain in entropy is the driving force for the adsorption of inhibitors on the MS surface [44].

The values of ΔH_{ads} and ΔS_{ads} can also be calculated by using following equation (10):

$$\Delta G_{ads} = \Delta H_{ads} - T\Delta S_{ads} \tag{10}$$

Using Eq. (10), the plot of ΔG_{ads} versus T gave a straight line (Fig. 7) with a slope of $-\Delta S_{ads}$ and intercept of ΔH_{ads}. The values obtained are well correlated with those obtained from Eq. (9), confirming the exothermic behavior of the adsorption of the studied inhibitors on MS in 0.5 M HCl.

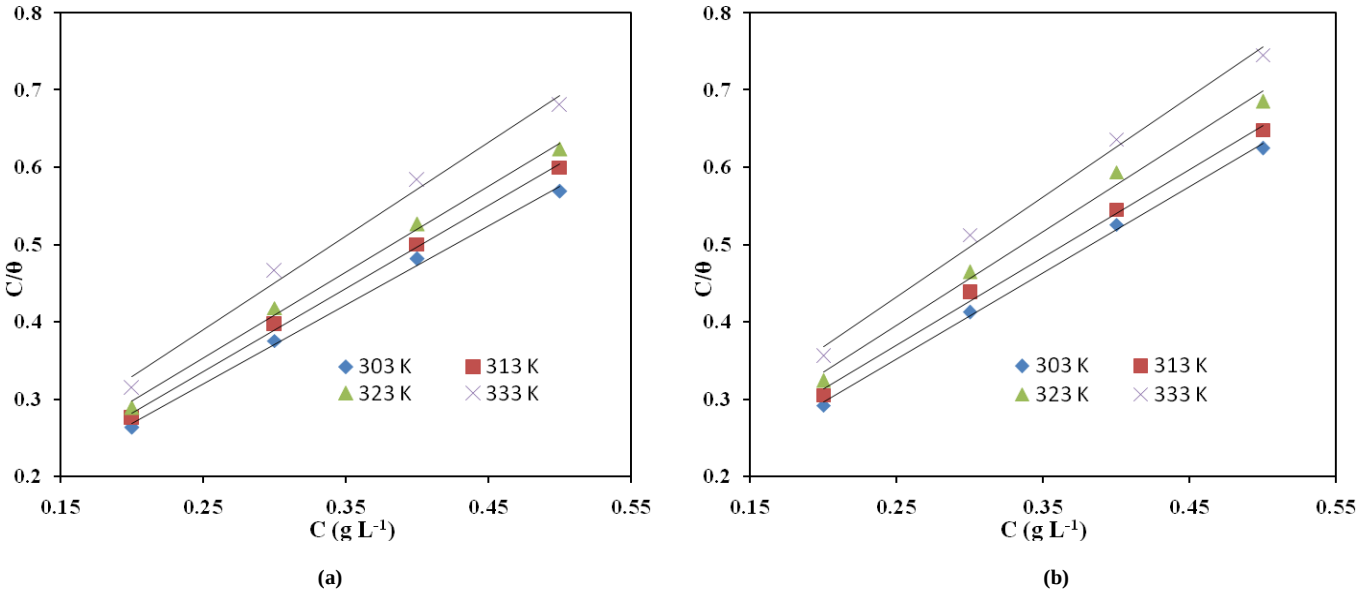

Figure 5. Langmuir adsorption isotherm on MS in 0.5 M HCl at different temperatures (a) 5a (b) 5b

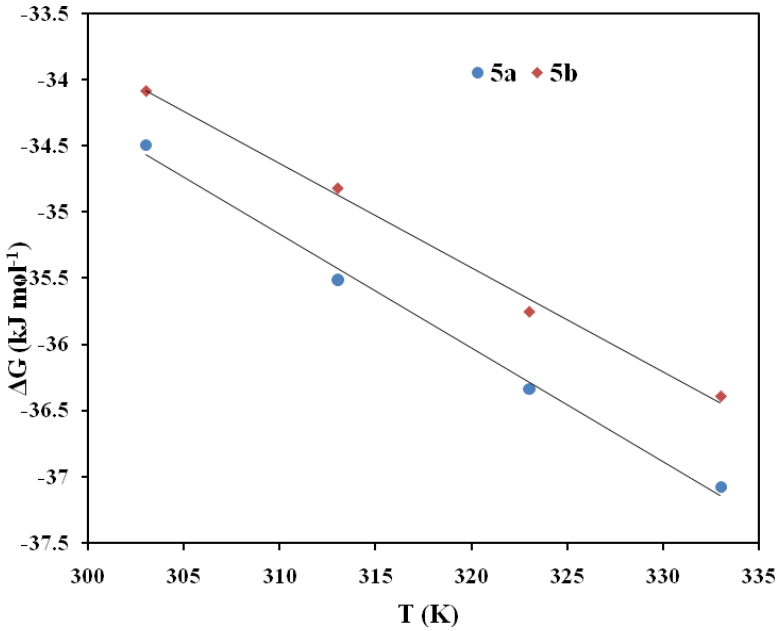

Figure 6. Plot of lnK_{ads} versus 1/T of compounds

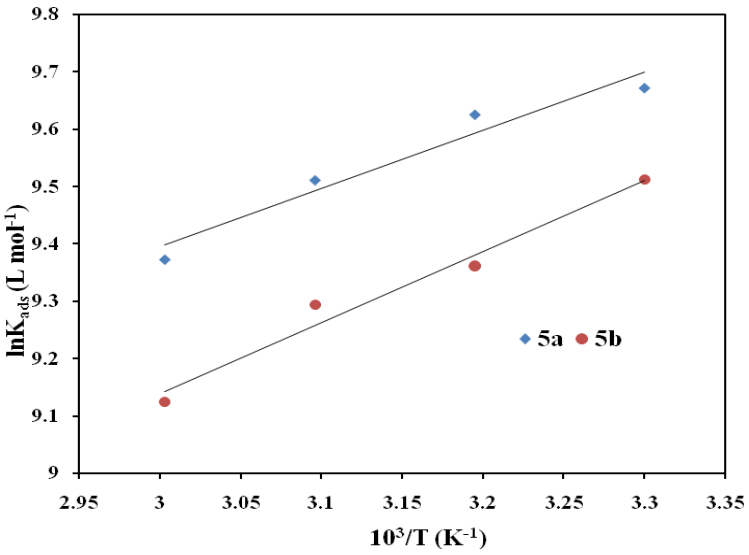

Figure 7. Plot of ΔG_{ads} versus absolute temperature

Table 4. Thermodynamic adsorption parameters for adsorption of 5a and 5b on MS in 0.5 M HCl at different temperatures from Langmuir adsorption isotherm

Inhibitor	Temperature (K)	slope	R^2	K_{ads} (L mol^{-1})	ΔG_{ads} (kJ mol^{-1})	ΔH_{ads} (kJ mol^{-1})	ΔS_{ads} (J mol^{-1}K^{-1})	$\Delta G_{ads} = \Delta H_{ads} - T\Delta S_{ads}$ (kJ mol^{-1})
5a	303	1.024	0.996	15873	-34.49			-34.30
	313	1.076	0.997	15151	-35.50	-8.43[a]	86.16[a]	-35.50
	323	1.113	0.995	13513	-36.33	-8.55[b]	86.00[b]	-36.33
	333	1.216	0.990	11764	-37.07			-37.07
5b	303	1.113	0.998	13513	-34.08			-33.96
	313	1.136	0.996	11627	-34.81	-10.29[a]	78.47[a]	-34.74
	323	1.212	0.991	10869	-35.74	-10.33[b]	78.00[b]	-35.74
	333	1.294	0.993	9174.3	-36.38			-36.38

[a] *Values obtained from Eq. (7)*
[b] *Values obtained from Eq. (8)*

3.6. Electrochemical impedance spectroscopy

The corrosion of MS in 0.5 M HCl solution in the presence of **5a** and **5b** was investigated by EIS method. Nyquist plots in the absence and presence of the inhibitors are presented in Fig. 8a and 8b. It is apparent that all Nyquist plots show a single capacitive loop, both in uninhibited and inhibited solutions. The impedance data of MS in 0.5 M HCl are analyzed using the equivalent circuit shown in Fig. 9, which includes the solution resistance (R_s), polarization resistance (R_P) and double layer capacitance (C_{dl}). The experimental results of EIS measurements for the corrosion of MS in 0.5 M HCl medium in the absence and presence of **5a** and **5b** are given in Table 5. Inspection of the Table 5 shows that R_P values increased with the increasing concentrations of the inhibitors. On the other hand, the values of C_{dl} decreased with increase in the inhibitors concentration. This situation was the result of an increase in the surface coverage by the inhibitor, which led to an increase in the η(%). The decrease in the C_{dl}, which can result from a decrease in local dielectric constant and/or an increase in the thickness of the electrical double layer, suggest that the compounds **5a** and **5b** function by adsorption at the metal/solution interface [45]. The R_P values increases as the inhibitor concentration is raised. This indicates that the resistance towards charge transfer reactions is responsible for corrosion process. These observations clearly prove the dependence of inhibitors concentration on corrosion control. The η(%) obtained from weight loss and electrochemical measurements are in good agreement with each other at all concentrations. It is seen that addition of inhibitor increases the value of R_P from 208.9 to 454.5 Ω cm^2 for compound **5a** and 157.5 to 278.3 Ω cm^2 for compound **5b**.

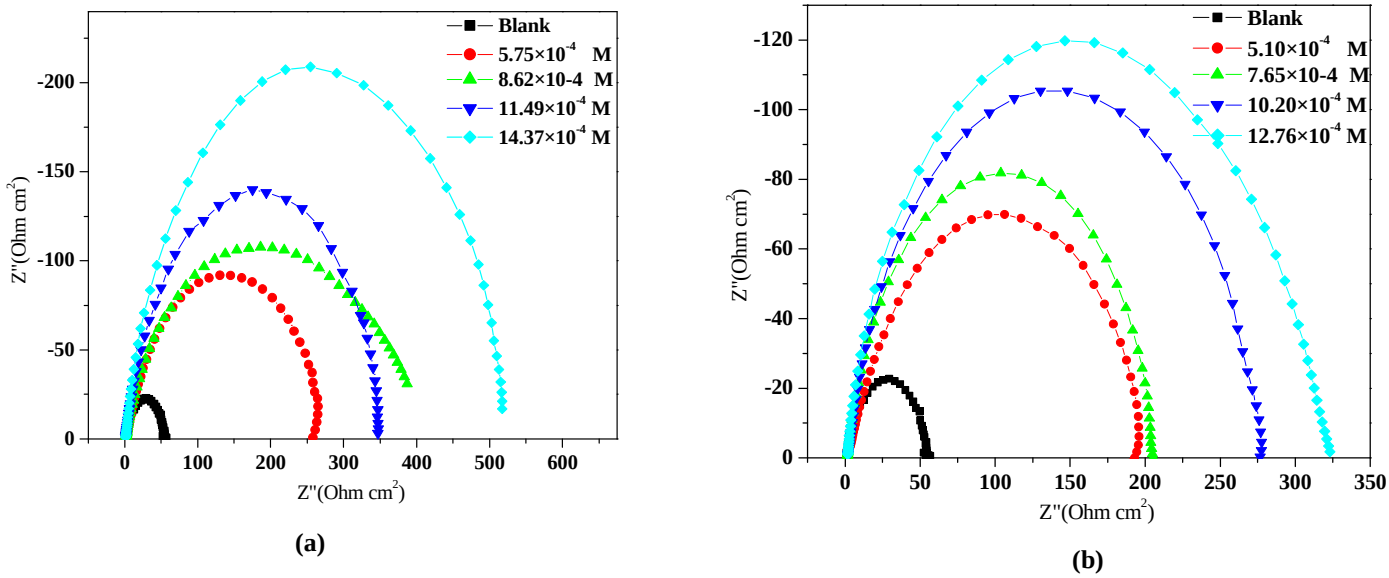

Figure 8. Nyquist plots for MS in 0.5 M HCl containing different concentrations of (a) 5a (b) 5b

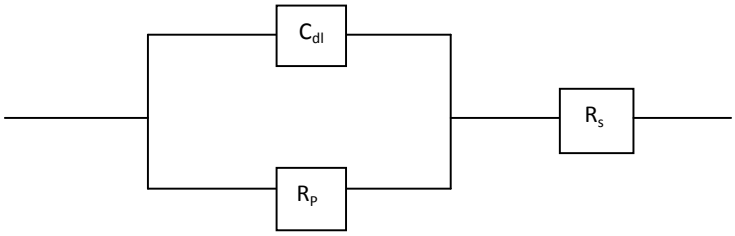

Fig. 9: Equivalent circuit diagram

Table 5. Electrochemical impedance parameters for MS in 0.5 M HCl in the absence and presence of different concentrations of 5a and 5b

Inhibitor	$C \times 10^{-4}$ (M)	R_P (Ω cm^2)	C_{dl} (μF cm^{-2})	η(%)
	0	50.02	76.12	
5a	5.75	208.9	54.15	76.05
	8.62	253.6	47.39	80.27
	11.49	303.2	40.93	83.50
	14.37	454.5	35.20	88.90
5b	5.10	157.5	55.18	68.24
	7.65	183.1	52.37	72.68
	10.20	237.8	48.28	78.96
	12.76	278.3	38.06	82.02

3.7. Potentiodynamic polarization measurements

The results of cathodic and anodic polarization measurements on MS in 0.5 M HCl solutions containing different concentrations **5a** and **5b** are shown in Fig. 10a and 10b as tafel plots. Inspection of the figures clearly indicate that the inhibitors **5a** and **5b** shifted both anodic and cathodic branches of Tafel curves to lower values of current density indicating that **5a** and **5b** acts as mixed type of inhibitors. This means, the addition of inhibitor molecules to HCl solution reduces the anodic dissolution of MS and also retards the cathodic hydrogen evolution reaction [46]. Increase in the concentration of **5a** and **5b** leads to shifting the corrosion potential to a more positive value relative to the blank. Both anodic and cathodic current densities obtained in 0.5 M HCl solutions in the presence of inhibitors

are lower than corrosion current densities obtained in the absence of inhibitors. The electrochemical polarization parameters obtained for **5a** and **5b** such as current density (I_{corr}), anodic (β_a) and cathodic (β_c) slopes and the corresponding η(%) values at different inhibitors concentrations were obtained by Tafel extrapolation at the corrosion potential (E_{corr}) are reported in Table 5.

Inspection of Table 5 clearly revealed that, the increase in inhibition efficiency η(%) is associated with a shift of both cathodic and anodic branches of the polarization curves towards lower current densities. Due to the presence of some active sites such as aromatic rings, hetero-atoms, the inhibitors act as adsorption inhibitors. Being absorbed on the metal surface, these compounds controlled the anodic and cathodic reactions during corrosion process, and their corrosion inhibition efficiencies are directly proportional to the amount inhibitors concentration. The η(%) values determined using polarization measurements are in good agreement with those obtained by EIS measurements.

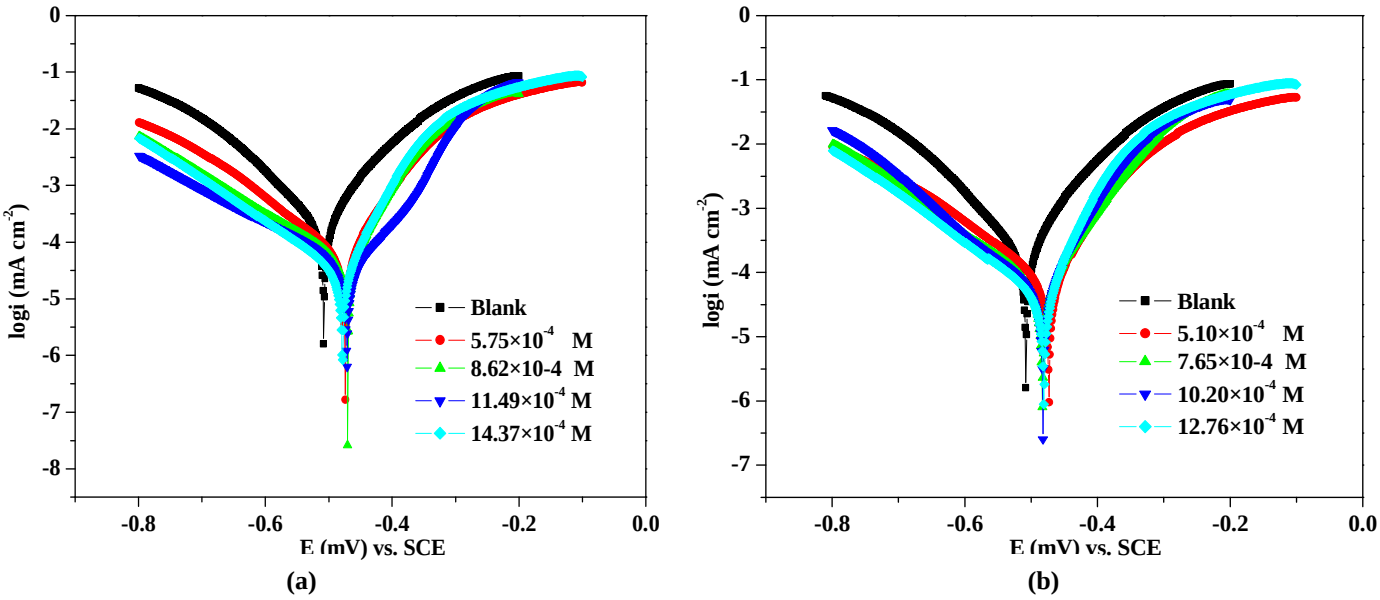

Figure 10. Potentiodynamic polarization curves for MS in 0.5 M HCl containing different concentrations of compounds (a) 5a (b) 5b.

Table 6. Electrochemical polarization parameters for MS in 0.5 M HCl in the absence and presence of different concentrations of 5a and 5b

Inhibitor	C×10^{-4} (M)	E_{corr} (mV)	I_{corr} (µA cm^{-2})	β_a (mA dec^{-1})	$-\beta_c$ (mA dec^{-1})	η(%)
	0	-0.508	261.7	11.28	8.73	
5a	5.75	-0.474	64.36	14.93	7.93	75.40
	8.62	-0.470	48.90	17.99	6.37	81.31
	11.49	-0.471	39.62	14.26	5.70	84.86
	14.37	-0.478	30.70	19.77	7.47	88.26
5b	5.10	-0.473	82.81	13.91	7.02	68.35
	7.65	-0.483	67.98	13.75	6.58	74.02
	10.20	-0.482	52.69	16.81	7.51	79.86
	12.76	-0.481	43.20	20.12	6.96	83.49

3.8. Surface analyses

The formation of a protective film of inhibitors on the MS surface was further confirmed by SEM observations. Fig. 11a shows SEM image of the polished MS surface. Fig. 11b shows surface of the MS specimen after immersion in 0.5 M HCl solution for 4 hr, while Fig 11c and 11d show MS specimens after immersion in 14.95×10^{-4} M and 13.21×10^{-4} M of the inhibitors **5a** and **5b,** respectively. After exposure of MS surface to uninhibited solution, the increase in the number of pits is observed on the surface (Fig 11b). Fig. 11c and 11d show the protected MS surface

after the addition of inhibitors **5a** and **5b** to acid solutions. Hence **5a** and **5b** have strong tendency to adhere to the MS surface.

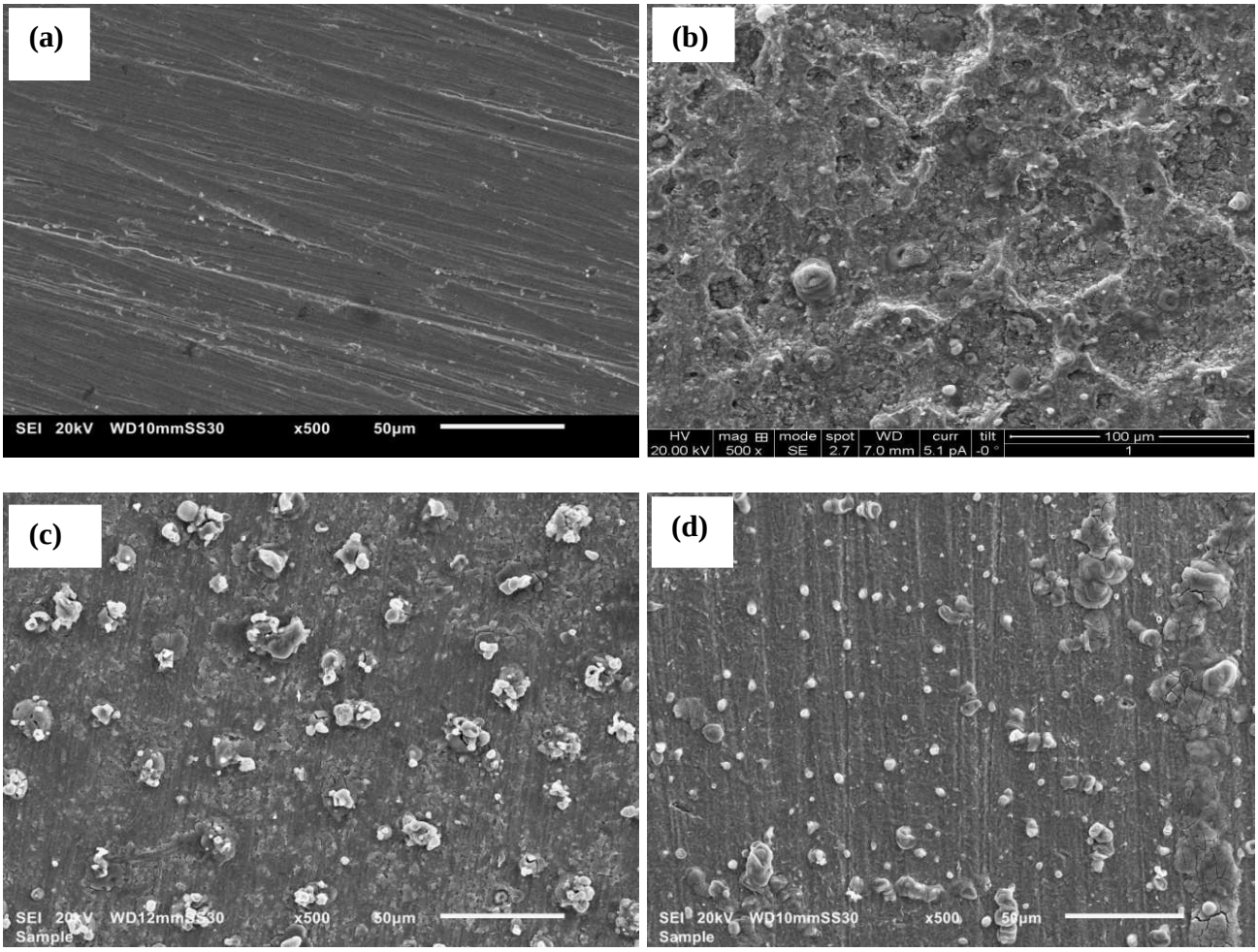

Figure 11. FTIR spectra of (a) pure 5a (b) surface film of the MS specimen after immersion in 0.5 M HCl containing 5a (c) pure 5b (d) surface film of the MS specimen after immersion in 0.5 M HCl containing 5b.

3.9. FTIR studies

FTIR is a powerful technique used to determine the type of bonding between the organic inhibitors and the metal ion. FTIR spectral analysis of the inhibitor film removed mechanically from the MS surface was carried out. Comparison of FTIR spectra of pure **5a** and **5b,** and inhibitors film removed mechanically from the MS surface was performed and given in Fig. 12a, 12b, 12c and 12d. It is seen from the FTIR spectra of inhibitor film mechanically removed from the MS surface that the intensity of the peaks are decreased and stretching frequencies are also decreased which implies that these compounds are coordinated to Fe^{+2} resulting in the formation of a Fe^{+2}- inhibitor complex on the metal surface.

Fig. 12a illustrates the FTIR spectrum of the **5a.** The strong broad bands at 2548 and 3541 cm^{-1} are attributed to S-H and O-H stretching. The absorption band at 2924 cm^{-1} is related to -CH_2- asymmetrical stretching vibration. The bands at 1545 and 1458 cm^{-1} are assigned to C=C stretching vibrations. The band around 1044 cm^{-1} is the stretching vibration of C-O in oxadiazole ring. The band at 1662 cm^{-1} indicates the stretching vibration of C=N. Hence, it can be inferred that compound **5a** contains oxygen and nitrogen atoms in functional groups (O-H, S-H, C=N, C–O, C=C) and aromatic ring, which meets the general structural consideration of the corrosion inhibitors.

Fig. 12b illustrates the FTIR spectrum of the surface film scrapped from the MS specimen after 4 h immersion in 0.5 M HCl containing **5a**. Comparison of the FTIR spectrum of the pure **5a (**Fig 12a) indicates that the band corresponds to S-H at 2548 cm^{-1} was found to be disappear and O-H stretching frequency at 3541 cm^{-1} is slightly shifted to 3446 cm^{-1}. The -CH_2 asymmetrical stretching vibration was decreased from 2924 to 2881 cm^{-1}. The band at 1662 cm^{-1} corresponds to C=N stretching vibration is shifted to 1632 cm^{-1}. These observations clearly indicate the formation of the metal – inhibitor complex which is responsible for preventing corrosion.

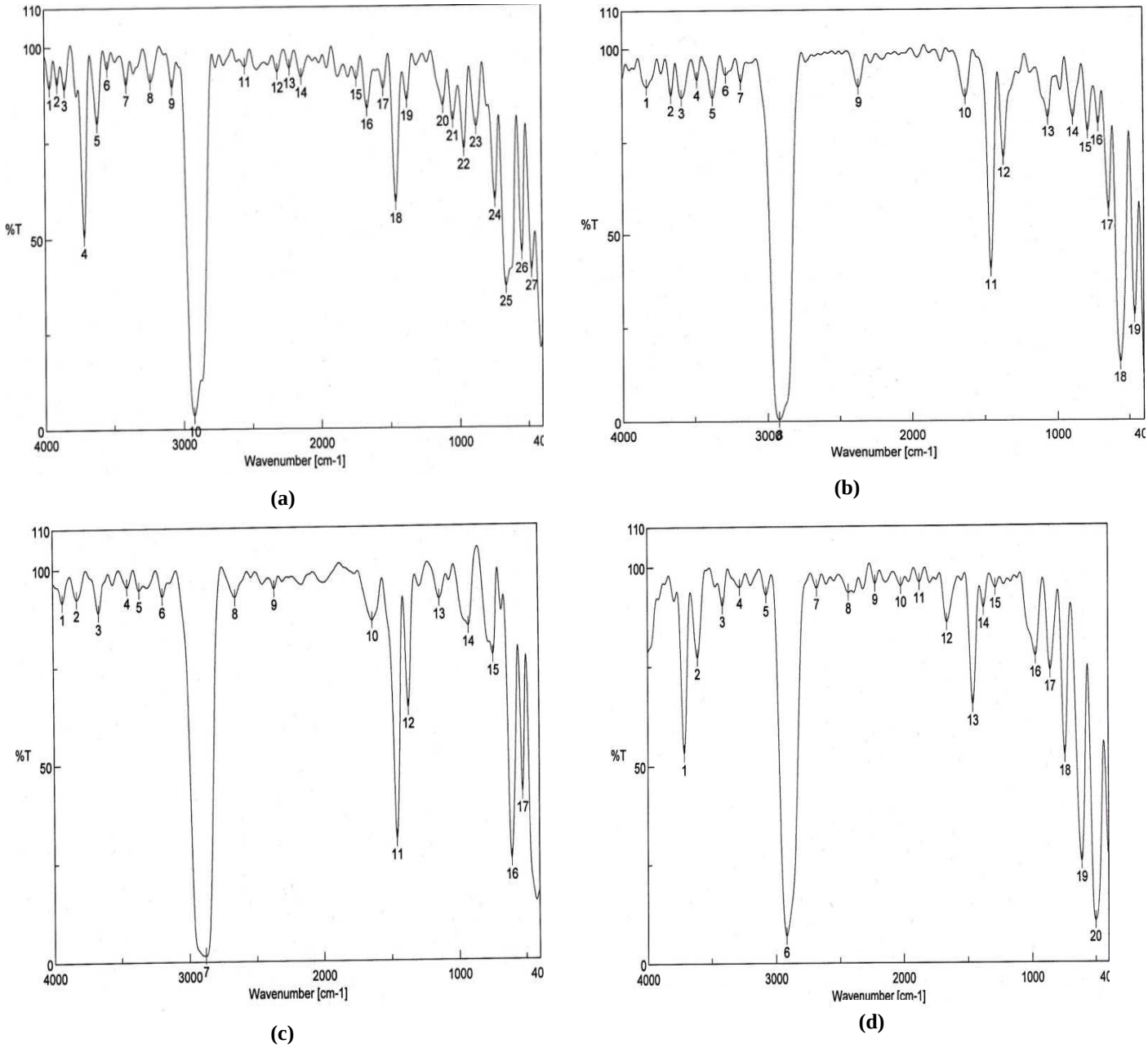

Figure 12. FTIR spectra of (a) pure 5a (b) surface film of the MS specimen after immersion in 0.5 M HCl containing 5a (c) pure 5b (d) surface film of the MS specimen after immersion in 0.5 M HCl containing 5b

CONCLUSION

Fig. 12c illustrates the FTIR spectrum of the pure **5b.** The strong broad bands at 2677 cm^{-1} and 3607 cm^{-1} are attributed to S-H and O-H stretching. The band at 1456 cm^{-1} are assigned to C=C stretching vibrations. A band around 1044 cm^{-1} is the stretching vibration of C-O in oxadiazole ring. The band at 1658 cm^{-1} indicates the stretching vibration of C=N. Hence, it can be inferred that compound **5b** contains oxygen and nitrogen atoms in functional groups (O-H, S-H, C=N, C-O, C=C) and aromatic ring, which meets the general structural consideration of the corrosion inhibitors.

Fig 12d illustrates the FTIR spectrum of the surface film on the MS specimen after 4 h immersion in 0. 5 M HCl containing **5b**. Comparison with the FTIR spectrum of the pure **5b (**Fig 12c) indicates that the band corresponds to S-H at 2677 cm^{-1} is found to be disappear and O-H stretching frequency at 3607 cm^{-1} is slightly shifted to 3586 cm^{-1}. The band at 1658 cm^{-1} corresponds to C=N stretching vibration is shifted to 1628 cm^{-1}. These observations clearly indicate the formation of the metal – inhibitor complex which is responsible for preventing corrosion.

The synthesized inhibitors **5a** and **5b** acted as potential corrosion inhibitors for MS in 0.5 M HCl. The percentage inhibition η(%) of designed molecules increases by increasing concentration, but it decreases with increasing temperature. The adsorption of the inhibitors on the MS surface follows Langmuir adsorption isotherm. The negative sign of the ΔH_{ads} indicates that the adsorption process is spontaneous and exothermic. The high K_{ads} values indicate a strong interaction between inhibitors and the metal surface. The polarization curves indicate that compounds **5a** and **5b** act as mixed type of inhibitors.AC impedance plots of MS indicate that charge transfer resistance increases with increase in inhibitors concentration. Morphological investigation by suggests that the addition of inhibitors in the aggressive solution results in the formation of the protective film on MS surface. FTIR results indicate the presence of a uniform and dense adsorptive film over the MS surface, which efficiently inhibits the corrosion of MS.

Acknowledgment
Authors would like to thank University of Mysore, Mysore, MHRD and UGC, New Delhi for providing financial assistance through Institution of Excellence (IOE) scheme.

REFERENCES

[1] W Durnie; B Kinsella; RD Marco; A Jefferson, *J. Electrochem. Soc.*, **1999**, 146, 1751-1756.
[2] F Bentiss; M Lagrenee; M Traisnel, *Corrosion*, **2000**, 56, 733-742.
[3] VS Sastri, Corrosion Inhibitors, Principles and Application, John Wiley and Sons, Chichester, UK, 1998.
[4] M Yadav; S Yadav, A Yadav, *J. Chem. Pharm. Res.*, **2011**, 3, 576-583
[5] MB Mahida; HG Chaudhari, *J. Chem. Pharm. Res.*, **2012**, 4, 5195-5201.
[6] DB Hmamou; MR Aouad; R Salghi; A Zarrouk; M Assouag; O Benali; M Messali; H Zarrok; B. Hammouti, *J. Chem. Pharm. Res.*, **2012**, 4, 3498-3504.
[7] BS Shylesha; T.V. Venkatesha, BM Praveen, *J. Chem. Pharm. Res.*, **2011**, 3, 501-507.
[8] MB Cisse; B Zerga; F El Kalai; ME Touhami; M Sfaira; M Taleb; B Hammouti; N Benchat; S El Kadiri; AT Benjelloun, *Surf. Rev. Lett.*, **2011**, 18, 303-313.
[9] AY Musa; RTT Jalgham; AB Mohamad, *Corros. Sci.*, **2012**, 56, 176-183.
[10] SE. Nataraja; TV Venkatesha; HC. Tandon, *Corros. Sci.*, **2012**, 60, 214-223.
[11] EA Noor, *Corros. Sci.*, **2005**, 47, 33-55.
[12] F. Bentiss; M. Lagrenee; M. Traisnel; JC. Hornez, *Corrosion.*, **1999**, 55, 968-976.
[13] MA Quraishi, FA Ansari, *J. Appl. Electrochem.*, **2006**, 36, 309-314.
[14] F Bentiss; M Traisnel; M Lagrenee, *Corros. Sci.*, **2000**, 42, 127-146.
[15] M Bouklah; B Hammouti; M Lagrenee; F Bentiss, *Corros. Sci.*, **2006**, 48, 2831-2842.
[16] F Bentiss; M Lagrenee, *J. Mater. Environ. Sci.* **2011**, 2, 13-17.
[17] MV Aanandhi; MH Mansoori; S Shanmugapriya; S George, P Shanmugasundaram, *Res J. Pharm. Biol. Che. Sci.*, **2010**, 1, 1083-1090.
[18] AA. Fadda; AAH Abdel-Rahman; WA. El-Sayed; TA; Zidan, FA Badria; *Chem. Heterocycl. Compd.*, **2011**, 47, 856-864.
[19] P Muthumani; R Meera; SB Agarwal; P Devi; *Int. J. Pharm. Biol. Arch.*, **2010**, 1, 338-344.
[20] F Bentiss; M. Lagrenee; M Traisnel; JC Hornez, *Corrosion*, **1999**, 55, 968-976.

[21] F Bentiss; M Traisnel; H Vezin; HF Hildebrand; M. Lagrenee, *Corros. Sci.*, **2004**, 46, 2781-2792.
[22] GW Kabalka; AR Mereddy, *Tetrahedron Lett.*, **2006**, 47, 5171-5172.
[23] S Tumkevicius; V Yakubkene; P Vainilavicius, *Chem. Heterocycl. Compd.*, **1999**, 35, 1334-1336.
[24] MC Hosur; MB Talawar; UV Lada, *Indian. J. Heterocycl. Chem.*, **1994**, 3, 237-242.
[25] MS Blois, *Nature*, **1958**, 181, 1199-1200.
[26] B Halliwell; JMC Guttridge; OI Aruoma, *Anal. Biochem.* **1987**, 165, 215-219.
[27] DC Garrat, Chapman and Hall ltd, Japan, **1964**, 3, 456.
[28] T Kochikyan; M Samvelyan; E Arutyunyan; V Arutyunyan; A Avetisyan; M. Malakyan; L Vardevanyan; S Badzhinyan, *Pharm. Chem. J.* **2011**, 44, 3-6.
[29] EA Shalaby; SMM Shanab; V Singh, *J. Med. Plants. Res.*, **2010**, 4, 2622-2632.
[30] FMA Elalla; EA Shalaby, *Aust. J. Basic & Appl. Sci.*, **2009**, 3, 3179-3185.
[31] F Mansfeld, *Electrochim. Acta*, **2007**, 52, 7670-7680.
[32] M. Schorr, J. Yahalom, *Corros. Sci.*, 1972, 12, 867-868.
[33] M Abdallah, *Corros. Sci.*, **2002**, 44, 717-728.
[34] KF Khaled; OA Elhabib; A El-mghrabya; OB Ibrahim; MAM Ibrahim, *J. Mater. Environ. Sci.*, **2010**, 3, 139-150.
[35] SS Abd El-Rehim; SAM Refaey; F Taha; MB Saleh; RA Ahmed, *J. Appl. Electrochem.*, **2001**, 31, 429-435.
[36] MA Quraishi; S Khan, *J. Appl. Electrochem.*, **2006**, 36, 539-544.
[37] A Yurt; G Bereket; A Kivrak; A Balaban; B Erik, *J. Appl. Electrochem.*, **2005**, 35, 1025-1032.
[38] UJ Naik; VA Panchal; AS Patel; NK Shah, *J. Mater. Environ. Sci.*, **2012**, 3, 935-946.
[39] T Poornima; J Nayak; AN Shetty, *Chem. Sci. J.*, Vol. 2012: CSJ-69, 1-13.
[40] RSA Hameed, *Adv. App. Sci. Res.*, **2011**, 2, 483-499.
[41] XH Li; SD Deng; H Fu; GN Mu, *Corros. Sci.*, **2008**, 50, 2635-2645.
[42] A Doner; G Kardas, *Corros. Sci.*, 2011, **53,** 4223-4232.
[43] G Moretti; G Quartarone; A Tassan; A Zingales, *Mater. Corros.*, **1994**, 45, 641-647.
[44] BG Ateya; BE El-Anadouli; FM El-Nizamv, *Corros. Sci.* **1984**, 24, 509-515.
[45] M Behpour; SM Ghoreishi; AG Niasar; N Soltani; MS Niasari, *J. Mater. Sci.*, **2009**, 44, 2444-2453.
[46] P Raja; M. Sethuraman, *Mater. Lett.*, **2008**, 62, 1602-1604.